

Momentum-dependent effects in $4f$ photoemission spectra from strongly correlated CeBe_{13}

A. B. Andrews, J. J. Joyce, A. J. Arko, and Z. Fisk*
Los Alamos National Laboratory, Los Alamos, New Mexico 87545

P. S. Riseborough
Polytechnic Institute of New York, Brooklyn, New York 11201
 (Received 13 June 1995)

We have studied the mixed-valent compound CeBe_{13} using a combination of high-resolution angle-resolved resonant photoemission and x-ray absorption. Based on the angle and temperature dependence of the intensity of the f^1 peak at the Fermi level, we conclude that the $4f$ state is most likely a narrow band with a bandwidth of ~ 50 meV, and may cross the Fermi level. The temperature dependence of the valence band photoemission spectroscopy can be accounted for by conventional thermal broadening effects. A mean valence of $\nu \sim 3.04$ is extracted from $M_{4,5}$ absorption spectra which agrees with L_{III} edge measurements, however the temperature dependence is negligible. A large amplitude anisotropy is observed in the f^0 peak, as well as about 0.1 eV of dispersion. Residual gas dosing in the submonolayer regime suggests that much of the f^0 intensity is surface related.

I. INTRODUCTION

The class of materials known as heavy fermions (usually compounds with an unfilled f shell) display macroscopic characteristics which suggest that the f electrons are generally localized with only a very weak interaction with the lattice.¹ Indeed, the prevailing model for heavy fermions is that the f electrons behave as noninteracting single magnetic impurities at high temperatures.^{2,3} However, because of slight residual hybridization with conduction electrons, they condense into a singlet state (with the conduction electrons) below a characteristic temperature, T_K . At still lower temperatures these impurities are presumed to form a periodic lattice⁴ which yields very narrow f bands whose width is of the order of T_K . The singlet f state is predicted to manifest itself as a very narrow density of states (DOS) near or just above the Fermi energy E_F , and is usually called the Kondo resonance, or KR (in the remainder of the paper we will often refer to this feature as the $4f_{5/2}$). It has very specific properties that should scale with T_K and should be measurable in a photoemission experiment. Indeed, the Gunnarsson-Schonhammer⁵ (GS) and the noncrossing approximation⁶ (NCA) predictions for photoelectron spectra in heavy fermions have served as guides to interpreting photoelectron spectra.

We have recently demonstrated⁷ with *in situ* prepared crystals of CePt_{2+x} ($x \leq 1$, $T_K < 20$ K), however, that not only does one *not* obtain the necessary scaling with T_K predicted by GS and NCA, but within the same crystal there occur large periodic intensity variations with crystal momentum in the $4f_{5/2}$ feature usually identified as the KR. Moreover, these intensity modulations, most easily explained as a small dispersion of a very narrow f band toward or above E_F , are observed at temperatures as high as 10 times T_K , far into the region where the magnetic susceptibility has a Curie-Weiss temperature dependence. This would seem to suggest band formation which is far more persistent than could possibly be explained by the Anderson lattice. The existence of this state

well into the Curie-Weiss regime demonstrates the lack of a temperature dependence that scales with T_K . Most unambiguously it shows that even at high temperatures we are not dealing with noninteracting single f impurities.

It is important to emphasize that at issue is not the existence of electron correlation effects in heavy fermion spectra. These unquestionably exist, as evidenced by the valence band satellites, extreme narrowness of the bands, and bulk thermodynamic properties. At issue is which of the prevailing models more correctly captures the physics of heavy fermion phenomena. Any successful theory must simultaneously predict the unusual macroscopic properties as well as the microscopic properties reported here, namely, the apparently bandlike and relatively temperature independent electronic structure. The prevailing single impurity model (SIM) is less successful with microscopic than with macroscopic properties. While it is sometimes speculated that even within SIM there may exist \mathbf{k} -dependent effects as observed by us, no calculations exist along these lines. Indeed, inasmuch as the KR results from an integration over all conduction band states,² it is difficult to envision directional effects.

In this paper we show that the amplitude modulation is universal in heavy fermion crystals by demonstrating that very similar results are obtained in both low- T_K materials (i.e., CePt_{2+x}) as well as those considered to be mixed valent (or large T_K , or sometimes referred to as α -like). We report detailed results of an angle resolved study of bulk single crystals of CeBe_{13} ($T_K \approx 400$ K) cleaved in vacuum and measured at the $4d$ absorption edge of Ce ($h\nu = 120$ eV). Besides the $4f_{5/2}$ amplitude effect we find unambiguous evidence for dispersion of the $4f_{7/2}$ peak, as well as anisotropy and dispersion in the main f^1 to f^0 transition at -2.4 eV. With 56 meV resolution we show unambiguously that the width of the $4f_{5/2}$ is at least three times larger than GS predictions even for this α -like material. CeBe_{13} is important toward an understanding of heavy fermion phenomena since, because of its relatively large T_K , it does not exhibit crystal field levels, and thus, within GS, the intensity at E_F can only

come from the KR for which NCA predicts a strong temperature dependence. Inasmuch as we show that no unconventional temperature effect is evident, it may be useful to consider alternate theories to SIM. In addition to renormalized band structure approaches, a recent theory by Sheng and Cooper⁸ may be promising.

CeBe₁₃ belongs to the class of intermediate valence (IV) compounds which exhibit an enhanced coefficient of the linear specific heat ($\gamma=115$ mJ K⁻²) (Ref. 9) and anomalous behavior in the lattice parameter. T_K is estimated to be between ~ 500 K based on susceptibility measurements⁹ and ~ 300 K from the quasielastic neutron scattering linewidth.¹⁰ Crystals of CeBe₁₃ were grown from an Al flux. Surface imperfections resulting from cleaving these crystals apparently do not totally average out the angular information, thus it is not always necessary to undergo the arduous task of *in situ* crystal growth to obtain sufficiently perfect crystals for angular studies. In the cubic NaZn₁₃ structure the Ce atoms are surrounded by a cage of Be atoms with no Ce-Ce nearest neighbors, so the material can be thought of as Ce atoms embedded in a Be host. Within the single impurity model, then, the f hybridization occurs primarily with the Be sp conduction band which is at least 10 eV wide.

The electronic structure of CeBe₁₃ has been the subject of a number of previous experimental and theoretical studies. The mixed-valent identity of CeBe₁₃ was ascertained by correlating lattice parameter measurements with changes in the x-ray photoemission spectroscopy (XPS) spectra.¹¹ The lattice parameter is anomalously low compared to other compounds in the LnBe₁₃ series.¹² Below 200 K the susceptibility is temperature independent suggesting a demagnetization of the Ce atoms.¹² The neutron scattering shows a quasielastic Lorentzian line shape.⁹ X-ray absorption at the L_{III} edge¹³ determined a valence of $v \sim 3.04$.

Self-consistent APW LDA (augmented plane wave-local density approximation) calculations¹⁴ show some degree of f band narrowing in CeBe₁₃ which is due to hybridization with the Be sp bands from below and Be p bands from above. The mixing with the host bands squeezes the f states more than in isostructural LaBe₁₃. However, the calculated mass enhancement is still too small by an order of magnitude to explain the specific heat and susceptibility data. Thus far "corrected" LDA calculations have not been attempted for CeBe₁₃ although it has been shown that such corrected LDA calculations¹⁵ can yield the experimentally measured values for UBe₁₃, a compound which has a mass enhancement ten-fold larger than CeBe₁₃.

Recently Lawrence *et al.*¹⁶ analyzed ultraviolet photoemission spectroscopy (UPS) spectra in terms of the GS model² and found that the calculated linewidth of the f^0 peak was at least three times larger than the experimental width. To date there have been no temperature dependent studies of the valence bands or $M_{4,5}$ x-ray absorption studies to complement existing L_{III} edge work.¹³ We might expect much larger temperature effects in CeBe₁₃ vs those reported for CeSi₂ (Ref. 17) ($T_K \approx 40$ K), based on the NCA predictions of scaling with T_K .

II. EXPERIMENTAL DETAILS

Photoemission measurements were done generally at the $4d$ - $4f$ resonance ($h\nu=120$ eV). The bulk of the data, with

resolution of 75 to 140 meV, was collected on the Los Alamos U3C beamline at NSLS, while additional spectra with resolution of 55 to 70 meV were obtained on the AT&T U4B Dragon beamline. For measurements near E_F , $\pm 1^\circ$ angular resolution was employed so that the acceptance cone corresponds to $\approx 25\%$ of the Brillouin zone at 120 eV.

At resonance the $4f$ contribution to the photocurrent is enhanced by a factor of ~ 100 because of an interference¹⁸ between direct processes of the form $4d^{10}4f^3(5d6s)^3 + h\nu \rightarrow 4d^{10}4f^2(5d6s)^3 + \epsilon_k$ and indirect processes $4d^{10}4f^3(5d6s)^3 + h\nu \rightarrow 4d^94f^4(5d6s)^3$ which decay via a super-Coster-Kronig process ($N_{4,5}N_{6,7}N_{6,7}$) to the same final state as in the direct process. If the host metal valence bands contribute substantially to the photocurrent, as is frequently the case, then the $4f$ emission may be obtained by subtracting the spectrum off resonance (below threshold) from the spectrum on resonance. In CeBe₁₃ (see below) this subtraction is not necessary due to the low Be sp cross section at $h\nu=120$ eV. It appears however, as shown below, that the Ce resonance spectrum is complicated by a substantial contribution from Ce- $5d$ emission which decays via a Coster-Kronig process ($N_{4,5}N_{6,7}O_{4,5}$).

In situ fracturing of the small (≈ 2 mm on a side) as-grown crystals was used to prepare a clean single crystal surface of CeBe₁₃. It is not known if the material has a true cleavage plane. However, because of the surprisingly large momentum dependence of the data, there was significant cleave to cleave variation. The samples were cleaved either at $T=20$ K or 300 K in $5e-11$ Torr vacuum. Data were typically collected for 3–4 hours or until noticeable oxygen contamination was visible in the valence bands, at which time a fresh cleave was made. All the dispersion data on the (100) surface reported here was collected from a single cleave with no detectable deterioration of the surface. The large T_K for CeBe₁₃ precluded the possibility of performing the measurement far above T_K as in CePt_{2+x}, so that measurements were generally done at 20 K, except for temperature effects at 300 K. Efforts were made with low-energy electron diffraction (LEED) to ascertain the surface orientation, but, although sharp spots were visible, we were unable to determine the surface orientation in this manner. In order to establish the bulk orientation of the cleaved surface, we removed the sample from vacuum and utilized x-ray Laue techniques. The direction normal to the cleaved surface found by this method was typically either (100) or (110). Spectra with very distinct signatures are found along each direction. Consequently, we will refer to the very different spectra found for each surface as either [100] type or [110] type.

III. RESULTS

While it is the features within 0.5 eV of the Fermi energy that are of greatest interest, we first consider the entire valence band spectrum. Because of the relatively strong time dependence of the spectra with residual gas adsorption, it is necessary to first delineate which features are bulk related vs surface related, and what indeed is the line shape of the true bulk spectrum. Toward this end the section below is intended to show that it is the feature closest to E_F which appears to

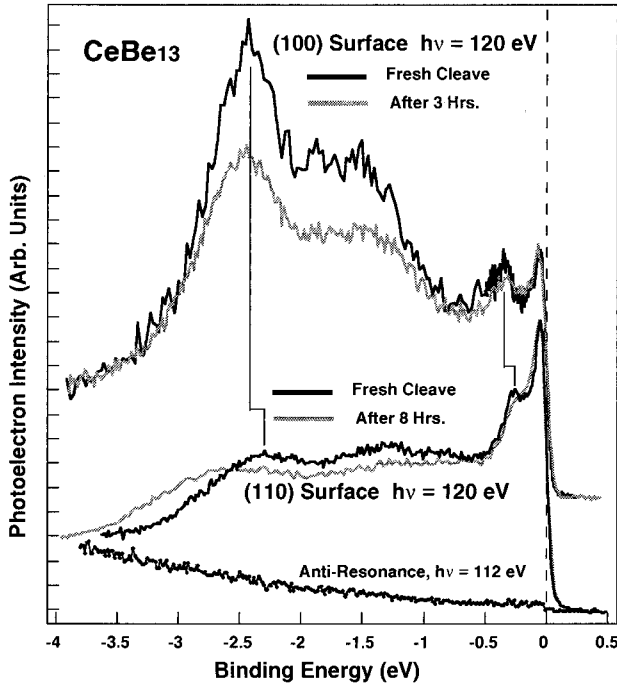


FIG. 1. Photoemission spectra for CeBe_{13} at $h\nu=120$ eV for the (100) and (110) surfaces. Dark lines correspond to fresh cleaves, while the gray scale lines correspond to data taken 3 and 8 hours after cleaving the (100) and (110) surfaces, respectively. Also shown is the spectrum at antiresonance ($h\nu=112$ eV) which is nearly featureless. Note the relative shifts in the f^0 and $4f_{7/2}$ features for the two directions.

change least with residual gas adsorption. Having established that, the remaining sections deal with the near- E_F features.

A. Complete valence band spectrum and the effect of the surface

Figure 1 displays valence band spectra on two different surfaces of CeBe_{13} at normal emission, on and off resonance, and as a function of time relative to a fresh cleave at 20 K in a vacuum of 3.5×10^{-11} Torr. The spectra shown in Fig. 1 represent the extremes observed representative of (100) and (110). (Any given cleave may also represent a combination of these two extremes, but we ignore these.) The beryllium s - p DOS (density of states) measured off resonance ($h\nu=112$ eV) obviously makes a negligible contribution to the total intensity at the $4d \rightarrow 4f$ resonance, allowing an unambiguous identification of the Ce $4f$ and $5d$ emission, and obviating the need for subtraction of the two spectra. The apparently increasing background intensity at antiresonance is due to the Be sp -DOS which peaks at -8 eV, plus the tail of a broad Be ($KL_{2,3}L_{2,3}$) Auger feature at a kinetic energy of ≈ 100 eV which does not interfere at $h\nu=120$ eV. In the region of interest, we can consider the Be contribution as negligible.

In Fig. 1 the dark line spectra correspond to fresh cleaves (the larger statistical noise results from the shorter counting times used to insure a proper representation of a clean surface), while the gray scale line spectra were taken 3 and 8 hours respectively after a cleave for the [100] and [110] di-

rections. For a given cleave (and emission angle) the spectra are normalized to the feature at E_F after it was ascertained that flux normalization yields nearly the same result. Normalization between different cleaves is more difficult, but it appears that the valley at ≈ -0.6 eV as well as the secondary background come closest to being the common points between all spectra, based on an average of many flux normalizations.

All spectra at resonance show at least 4 distinct features attributable to Ce emission. The $4f$ emission consists of the three-peaked structure including the broad peak at ≈ -2.3 to -2.4 eV (depending on orientation), and two narrow features near the Fermi energy. This is a characteristic feature of all Ce compounds and is well documented in the literature.^{17,20} The structure at ~ -2.4 eV is the so-called “main” peak associated with the transition $4f^1 \rightarrow 4f^0$ while the two peaks at the Fermi level are commonly identified in the literature^{3,17} as the KR ($E_B \sim -0.03$ eV) and its associated spin orbit sideband ($\Delta_{S.O.} \sim -0.3$ eV). The features between -0.5 and -2 eV derive from Ce- $5d$ emission as clearly demonstrated from the cross section dependence at lower photon energies (not shown). The $5d$ emission features likewise undergo a dramatic intensity enhancement at the $4d$ absorption edge (verified on LaBe_{13}) despite the fact that the Auger process is only Coster-Kronig and not super-Coster-Kronig. The enhancement appears to be about 50% of the peak f -emission intensity,¹⁶ but normalization is difficult.

A striking anisotropy is observed in normal emission between spectra from the (100) and (110) surfaces in all features, in position as well as intensity. If the Fermi energy is placed at the midpoint of the Fermi edge, then all features (except the $4f_{5/2}$) in the [100]-type spectra are about 50 to 100 meV higher in binding energy relative to the [110]-type spectra. Note that the [110] spectrum apparently yields two $5d$ features, while only one broad $5d$ peak is resolved in [100] spectra.

Next we address the time dependence seen in the spectra of Fig. 1 even at 20 K and a vacuum of 3.5×10^{-11} Torr, which is interpreted as a suppression of the surface contribution to spectrum and a growth of surface oxide. One of the reasons cited for the poor agreement with the GS model calculations has been the surface sensitivity of the UPS technique,^{19,20} which samples only the top few layers of the compound. Unlike Yb compounds,²¹ where the surface components of the (divalent) $4f$ signal are easily distinguished by a large surface/bulk splitting ≈ 0.9 eV, the size of the surface/bulk splitting is too small to be distinguished in Ce compounds. It is well known that the surfaces of a number of rare-earth metals (e.g., Sm) as well as numerous compounds undergo valence transitions at the surface. This phenomenon is understood as a decreased coordination at the surface which makes it more favorable in some cases to adopt a more atomiclike valence. In the case of Ce, it has been noted^{19,20} that the surface layers of α -Ce and some “ α -like” Ce compounds (or large T_K) are “ γ -like” (more trivalent) based on the observation that the relative f^0 spectral weight decreases with increasing kinetic energy. The precise depth of the surface region is unknown, but our dosing experiments indicate no more than the top layer. If progress is to be made, the surface contribution must first be identified.

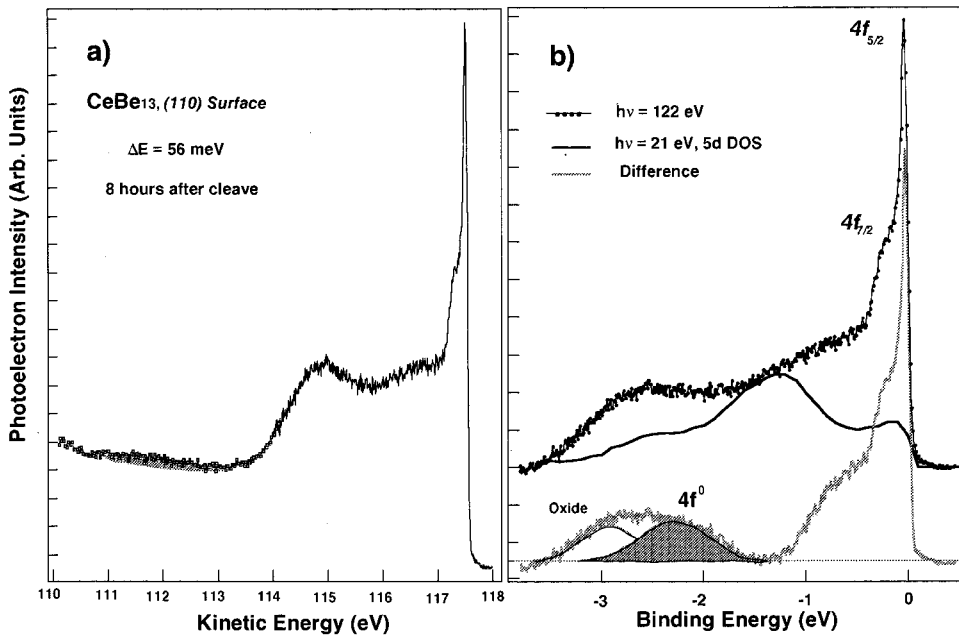


FIG. 2. (a) Spectrum at $h\nu = 122$ eV and at 56 meV resolution for the same (110) surface as in Fig. 1 (after 8 hours). The miniscule oxygen contamination is shown as the shaded area. (b) Same spectrum as in (a) but with an integral background subtracted. The solid dark line is the 5d-electron spectrum as obtained at $h\nu = 21$ eV. Subtraction of the two spectra yields the gray scale spectrum at bottom. The shaded f^0 peak has been fit with a Gaussian at the position of the fresh cleave. Note the new oxide feature growing with time.

The data of Fig. 1 clearly show that the f^0 peak is decreasing with time relative to the $4f_{5/2}$ due to submonolayer adsorption of gases, suggestive of a surface contribution to the spectrum. The decrease is much smaller along [110] which might suggest that here the effect of the surface is less pronounced and that the position and size of the f^0 peak may be more correctly representative of the bulk. Careful oxygen dosing experiments²² for a (100)-type surface have shown that the f^0 peak first decreases up to an oxygen dosing of ≈ 0.2 L, and then begins to broaden, shift toward higher binding energy, and again increase in intensity with the formation of a surface oxide. Because of these changes the intrinsic line shape of the f^0 peak remains undetermined. The spectra in Fig. 1 correspond to a surface dosing of no more than 0.1 ± 0.05 L. Surprisingly, the $4d$ features at ≈ -1.5 eV likewise show dosing dependence, with shifts evident even at small dosing. By contrast, the $4f_{5/2}$ shows almost no intensity decrease up to a dosing of 0.2 L, and prior to the shifting of the f^0 peak. It is justified, then, to associate the $4f_{5/2}$ with a primarily bulk feature. While the intrinsic bulk intensity of f^0 is difficult to ascertain, for the purposes of this paper we will call the intensity along [110] as the intrinsic bulk intensity despite the surface effects and the fact that a strong anisotropy is evident in the data, and that indeed we cannot exclude the possibility that the bulk f^0 intensity may be identically zero for some directions of the crystal. The $4f_{7/2}$ peak for the [100] direction and to a much lesser extent for the [110] direction, also shows dosing dependence of the amplitude relative to the $4f_{5/2}$. Perhaps here too there is a small surface contribution, but less pronounced than for the f^0 peak.

The (110) spectrum of Fig. 1 (8 hours after cleaving) was repeated with 56 meV resolution and is shown in Fig. 2(a). The spectral features at kinetic energies between 110 and 114 eV (taken with lower resolution) show the almost insignificant oxygen contribution (shaded area) which nevertheless is sufficient to change the f^0 feature. In Fig. 2(b) the same spectrum is displayed, but with the secondary background subtracted via the standard integral background method.

An approximate line shape of the of the 5d-electron spectrum can be obtained by using lower photon energies where the 4f cross section is negligible. Figure 2(b) displays one such line shape obtained at 21 eV. But it must be noted that the line shape can change with photon energy and emission angle. In view of the surface and angle dependence of this emission, a complete study of the 5d spectrum was deemed beyond the scope of this paper. LaBe₁₃ was measured at resonance, but while the shape of the spectrum was very similar to that shown in Fig. 2(b) [lending confidence as to the correctness of the 5d spectrum in Fig. 2(b)], the peaks were shifted in energy relative to CeBe₁₃. Moreover, while the line shape can be measured, normalization to the spectrum at resonance is still difficult. However, it should be emphasized that before a direct comparison can be made to GS or NCA, just such a normalization and subtraction of the 5d must be made, otherwise the experimental 4f line shape is meaningless. Several normalizations were made which, when compared to a GS calculation, consistently suggest a Ce valence far in excess of the 3.04 measured in XAS (see below). One such normalization and subtraction is shown in Fig. 2(b) which seems plausible, although we admit that it is somewhat arbitrary. The difference spectrum, however, will always have approximately the shape shown. The f^0 peak is shaded in the figure in order to more clearly demonstrate the growth of surface Ce oxide at the 0.1 L level. Needless to say, a similar analysis along (100) produces an entirely different spectrum.

B. The amplitude modulations of the $4f_{5/2}$ peak

Figure 3 shows spectra in the near- E_F region for several different angles on a (100) surface taken within 2 hours of each other on the same cleave (our flattest cleave which was also the most stable with time, showing no deterioration during measurement). After 2 hours all data were repeated again and found to reproduce almost exactly. While the actual direction of k_{\parallel} is not established, it is obvious that the $4f_{5/2}$ does not have a constant amplitude throughout the Brillouin

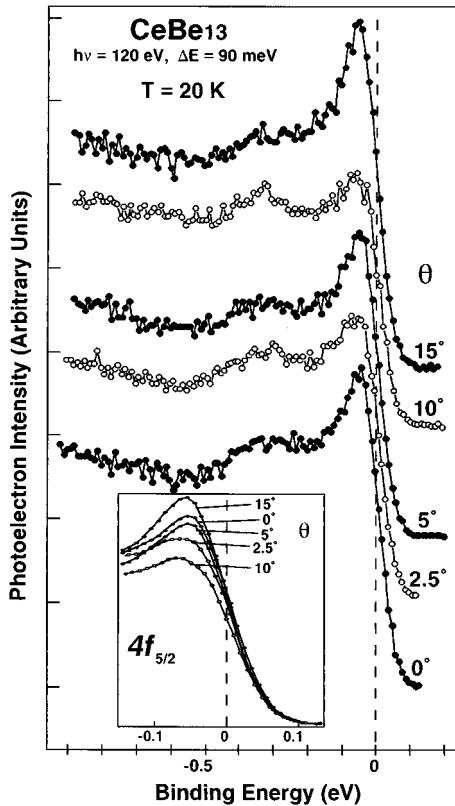


FIG. 3. Near- E_F spectra at resonance from a (100) surface as a function of angle, θ . Note the periodic amplitude modulations of the $4f_{5/2}$ feature. The inset shows the same spectra but now superimposed and slightly smoothed to emphasize the amplitude effect.

zone (BZ) as one would expect from the SIM. Indeed the amplitude modulations exhibit periodic behavior consistent with itinerant states. The inset shows the same spectra, but now smoothed with a 50 meV Gaussian (much less than our resolution) and plotted on top of each other to emphasize the periodic amplitude effect. These amplitude modulations are observed only when $\pm 1^\circ$ angular resolution is employed. Evidently this is because the larger $\pm 4^\circ$ aperture simply averages out these intensity modulations. Even a $\pm 1^\circ$ aperture still averages over $\approx 25\%$ of the BZ (in all directions) compared to nearly 100% for the $\pm 4^\circ$ aperture. We have seen similar behavior in many of the single crystal compounds we have studied.^{7,23} The period of the amplitude oscillations, which we interpret as approximately the Γ - Γ distance, is $8^\circ \pm 1^\circ$ corresponding to $0.6 \pm 0.08 \text{ \AA}^{-1}$, while $2\pi/a = 0.61 \text{ \AA}^{-1}$ for cubic²⁴ CeBe₁₃. In Fig. 3 the minimum $4f_{5/2}$ intensities occur at 2.5° and 10° which are associated with approximately the Γ points. The spectrum closest to a zone boundary (presumably a [110] direction) then is the 15° spectrum which also has the largest $4f_{5/2}$ intensity. Indeed, this spectrum has the greatest resemblance to a spectrum (see Fig. 5 below) taken at normal emission from a (110) surface. The two spectra need not be identical since in a three dimensional crystal the 25% of the zone sampled by the finite angular aperture is entirely different for the two directions. From the relative intensity variations between the $4f_{5/2}$ and the $4f_{7/2}$ we rule out photoelectron diffraction as the mechanism for the modulations.

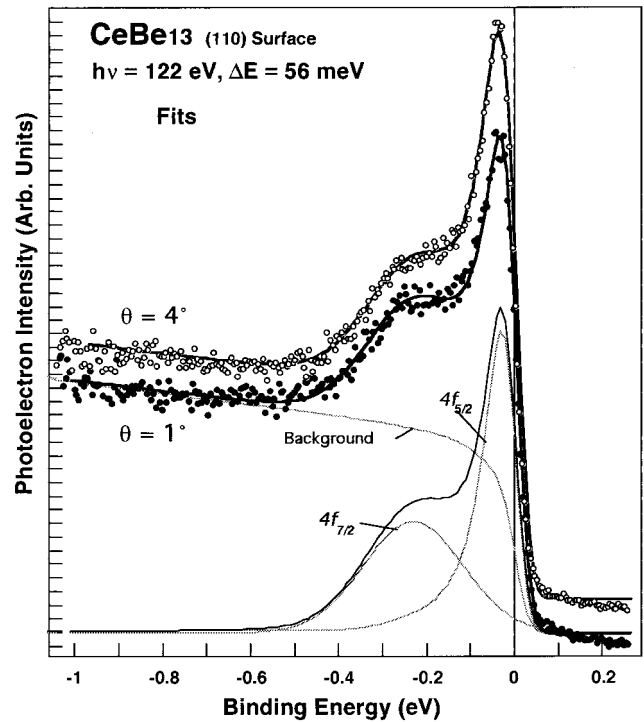


FIG. 4. Line shape analysis of two spectra from a (110) surface at $h\nu = 122 \text{ eV}$ and 56 meV resolution, with takeoff angles of 1° and 4° relative to the surface normal. The fitted $4f_{5/2}$ shifts by 17 meV between the two spectra, all other parameters remaining fixed. The fitting components are shown for the $\theta = 1^\circ$ spectrum (see text for parameters).

As suggested before, a very plausible explanation for the amplitude modulation is a dispersion of the narrow $4f_{5/2}$ band toward E_F . However, even the 56 meV resolution in this study is insufficient to see a dispersion of 25 meV if, as is the case for this data, the feature occurs within 25 meV of the Fermi energy. Modeling of the spectra has shown that the position of the $4f_{5/2}$ peak with respect to the midpoint of the Fermi edge will be primarily a function of the resolution whenever the latter exceeds the dispersion by a factor of 2 or more. Thus for a given resolution the $4f_{5/2}$ peak will appear at about the same apparent binding energy irrespective of dispersion. Its amplitude, however, will vary as shown below. Surface lifetime considerations prevented us from obtaining reference spectra for each angle, but fits to the data indicate that for our highest resolution data, $\approx 56 \text{ meV}$ to $\approx 70 \text{ meV}$, the Fermi energy is near the midpoint of the Fermi edge, while for data with $\approx 100 \text{ meV}$ resolution, the Fermi energy is about one third of the way down from peak height.

The dispersion hypothesis was tested by fitting the data at different angles. In Fig. 4 we show typical fits to our highest resolution data, obtained on a (110) surface [despite the fact that in the (110) plane the maximum amplitude variation is only about 15%]. The high resolution allows an unambiguous determination of the intrinsic peak width which is critical in any comparison to GS or NCA. The main unknown quantity in the fits is the exact line shape of the $5d$ spectrum near E_F which must first be subtracted out to get the $4f$ spectrum. The approximate shape in the [110] direction is known from

Fig. 2, but intensity is not known to better than a factor of 2. As a result, the background, as shown in Fig. 4, is somewhat arbitrary, but similar to other heavy fermion analyses. This version of the background tends to underestimate the width of the $4f_{5/2}$ (this is simply because too much spectral weight is put into the background, thus cutting off the bottom portion of the Lorentzian), and thus yields a lower limit on this linewidth, which, as we see below, is already larger than GS predictions. In Fig. 4 we used a Lorentzian line shape for the $4f_{5/2}$ and a Gaussian line shape for the $4f_{7/2}$ peak (it was experimentally determined that the Gaussian line shape yielded a better approximation of the $4f_{7/2}$). For both directions shown, the full width at half maximum (FWHM) of the Lorentzian is 100 meV while that of the Gaussian (located at -230 meV in both spectra) is 320 meV. Since our resolution is 56 meV, the line shapes are essentially unaffected by instrument broadening. The only difference between the fits for the two directions is that at $\theta=1^\circ$ the Lorentzian is centered at -6 meV, while for $\theta=4^\circ$ the Lorentzian has been shifted to -23 meV. All other parameters are identical, despite the fact that there is no *a priori* reason to keep them identical. Thus the 15% amplitude modulation of the $4f_{5/2}$ on the (110) surface is easily and completely explained by 17 meV of dispersion of the $4f_{5/2}$. If one works within the GS or NCA models, the lower limit of 100 meV for the intrinsic FWHM corresponds to a T_K of 1200 K as compared to ≈ 400 K measured from bulk properties.

As we have often emphasized,^{7,25} one can obtain good fits to the data with other combinations of parameters, backgrounds and line shapes (e.g., Doniach-Sunjc line shape for the $4f_{5/2}$ and Lorentzian for the $4f_{7/2}$). We have looked into this, but the basic physics of dispersion does not change. In particular, one can use an integral background with the assumption that all intensity at ≈ -1 eV is due to secondary electrons. In this case the background intensity approaches zero near E_F thus putting maximum spectral weight into the $4f$ features. Using this background one gets an upper bound of 140 meV for the $4f_{5/2}$ FWHM (corresponding to a $T_K \approx 1680$ K) for the spectra of Fig. 4, which is identical to the value we obtained²⁶ in our similar analysis of the CeSi₂ ($T_K \approx 35$ K) spectra of Patthey *et al.*,¹⁷ and first reported²⁷ at the March Meeting in 1991. Thus there is absolutely no difference in the intrinsic widths of the $4f_{5/2}$ peaks for materials whose actual T_K 's differ by an order of magnitude, nor is higher resolution needed to determine the linewidths.²⁸ Higher resolution may still be useful to see dispersion of the $4f_{5/2}$ without line shape analysis provided that much smaller acceptance cones are used to zoom in on a smaller portion of the Brillouin zone.

Having established the intrinsic linewidth, we next address by quantitative data reduction the more substantial (100) surface dispersion. In Fig. 5 we show fits to the 10° and 15° spectra of Fig. 3, using similar line shapes and widths obtained in Fig. 4. The position of the $4f_{5/2}$ Lorentzian for the 15° spectrum, however, is at -30 meV rather than -23 meV obtained in the (110) data. Recall that we are sampling a rather different 25% of the Brillouin zone. The 10° and 15° spectra were taken within minutes of each other with no changes in instrument settings except analyzer angle. Moreover, they were repeated after several hours and found to reproduce very closely. The instrument broadening for the

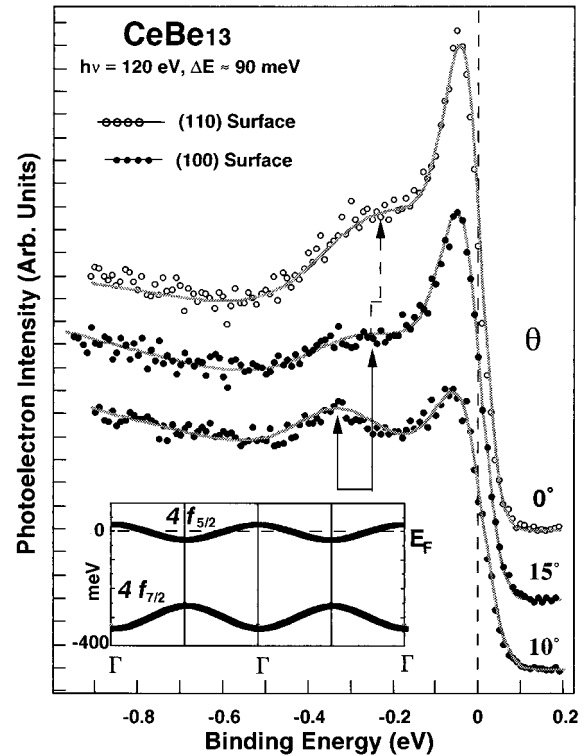


FIG. 5. Line shape analysis of the 10° and 15° spectra of Fig. 3, as well as a spectrum from a (110) surface at 90 meV resolution for comparison. A 50 meV shift of the $4f_{5/2}$ is needed to explain the amplitude effect (see text). The shift of the $4f_{7/2}$ is seen unaided, with the arrows pointing to the fitted positions of the $4f_{7/2}$ (a shift of up to 90 meV). Inset shows a schematic of the fitted dispersion of the $4f_{5/2}$ and $4f_{7/2}$ features in CeBe₁₃.

data in Fig. 5 is nominally 90 meV. For comparison we also show a spectrum taken at normal emission on a (110) surface with the same instrument broadening of 90 meV in order to emphasize its resemblance to the spectrum at 15° (for this [110] spectrum the fitting parameters are identical to the $\theta=4^\circ$ spectrum in Fig. 4, except for instrument broadening). The important things to note regarding the fits are the following. (1) To obtain a fit to the 10° spectrum it was necessary to shift the $4f_{5/2}$ from -30 meV (in the 15° spectrum) to $+20$ meV and broaden it somewhat (from FWHM=90 meV to 150 meV), thus yielding a total dispersion of 50 meV. (2) The dispersion in the $4f_{7/2}$ peak is visible by eye without the aid of fits. The fitted positions of the $4f_{7/2}$ peak are marked by arrows in Fig. 5 and range from -250 meV for the 15° spectrum to -325 meV for the 10° spectrum, while the Gaussian FWHM decreases from 320 meV to 220 meV, respectively. (3) For the (110) surface in Fig. 5, the fitting parameters are the same as in Fig. 4 so that the $4f_{7/2}$ peak is at -230 meV and the $4f_{5/2}$ is at -23 meV. Thus the dispersion of the $4f_{7/2}$ peak is between 75 and 95 meV, with a momentum dependence out of phase with the $4f_{5/2}$. If we postulate a Kondo lattice and assume that the dispersion is a measure of T_K , these values again correspond to a T_K as high as 1200 K.

The use of a Doniach-Sunjc line shape for the $4f_{5/2}$ as well as a Lorentzian line shape for the $4f_{7/2}$ primarily affects

the amplitude and width of the $4f_{7/2}$ peak. The centroid positions are only minimally changed from the above analysis.

A visual aid to the suggested band structure is shown by the inset in Fig. 5 with the primary aim of showing the strength and phase of the dispersion. It is of course, not intended to be correct in detail. We caution again that we are not observing a well defined quasiparticle state due to averaging over 25% of the zone. For this reason the dispersion values obtained represent an average, while the actual dispersion may be substantially larger (or smaller) in some directions.

C. Temperature dependence

As noted earlier, a number of groups have claimed to observe a temperature dependence in the spectral weight of the $4f_{5/2}$ [notably^{17,29} in CeSi_2 , but also in YbAl_3 (Ref. 30)], which is in agreement with predictions of finite temperature noncrossing approximation⁶ or NCA. Since the f occupancy is farther from unity in CeBe_{13} than in CeSi_2 , NCA predicts⁶ an even larger temperature effect in CeBe_{13} , particularly since crystal field complications are not present. In the course of our investigations we have discovered that temperature dependence is perhaps the most difficult parameter to utilize for comparison to theory since all materials display a temperature dependence to some degree. In addition, the time dependence discussed above can easily be mistaken for a temperature dependence. It is necessary to first separate out conventional temperature effects before assigning these to novel mechanisms. As a general rule, the narrower the peak, the larger the apparent conventional temperature dependence, particularly near E_F where the Fermi function dominates.

To study the temperature dependence of the $4f$ bands in CeBe_{13} we first consider the x-ray absorption spectroscopy (or XAS) which can be obtained in a photoemission experiment in the total yield mode; i.e., by measuring the secondary electron output as one tunes the photon energy through the $3d$ absorption edge. This technique is generally more bulk sensitive than resonance photoemission spectroscopy (PES) and has been considered by some as more model independent (although we would challenge that assumption).

Figure 6 shows the M_5 spectrum of CeBe_{13} at 20 and 300 K. The lack of temperature dependence is detailed below, but first we focus on extracting the valence. The spin-orbit splitting of the M_4 and M_5 is ~ 9 eV and thus the M_4 is not shown. The main peak has been attributed to a $3d^9 4f^2$ final state.³¹ The multiplet structure within the f^2 manifold is nearly washed out due to limited experimental resolution at 900 eV. The emergence of a second peak at ~ 5 eV higher energy is identified with a $3d^9 4f^1$ final state and is associated with increasing hybridization and decreasing f count. The transition energy for the process $i \rightarrow 3d^9 4f^2$ is ~ 5 eV lower than the energy for the process $i \rightarrow 3d^9 4f^1$ due to the difference in Coulomb correlation energies between the $4f$ subshell and the $3d$ core hole, $U_{fc} \sim 10$ eV, and the Coulomb repulsion of the f electrons $U_{ff} \sim 5$ eV. To extract the f occupancy (n_f) we first estimate the area of the smaller f^1 peak after subtracting a secondary background. The remainder then consists of the components of the f^2 multiplet. By this method we find that $I(f^1)/[I(f^1)+I(f^2)] = w(f^0) = c_f^0 \sim 0.04$ which gives us an estimate of the valence as

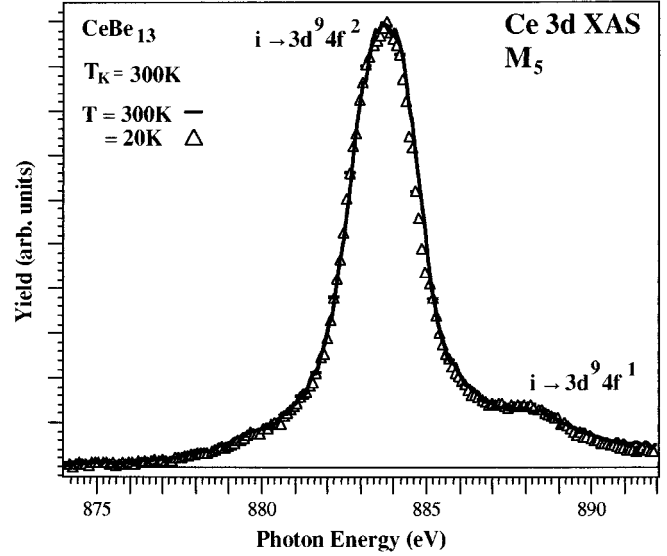


FIG. 6. The M_5 XAS spectra at the $3d$ edge taken in the total yield mode, at 20 K and at 300 K. There is no obvious temperature dependence in the f^1 feature.

$v = 3.04$ and $n_f = 0.96$. This value is in agreement with earlier estimates of 0.96 based on L_{III} absorption edge¹³ studies.

According to the NCA,⁶ n_f should decrease by $\sim 2\%$ between $T = 300$ and 20 K to a value of about 0.94. Therefore as the temperature is lowered we would expect the intensity of the f^1 component to increase by $\sim 30\%$ to 50% , since 2% of the area of the much larger f^2 peak added to f^1 should lead to a percentage increase of the smaller f^1 component by this amount. The lack of this expected intensity modulation cannot be blamed on surface effects since XAS is bulk sensitive, i.e., the electrons have been scattered many times and come from deep inside the crystal. This result appears to be in conflict with L_{III} edge analysis for other heavy fermion compounds,³² but is completely consistent with the PES which we discuss next.

In Fig. 7 we show the same spectrum as in Fig. 5 (open circles at 20 K) but now we also show the effect of raising the temperature to 300 K (filled circles). At first glance there appears to be a substantial temperature dependence at odds with the XAS discussion immediately above. However, one must consider normal temperature effects such as Fermi function dependence and phonon broadening. The bulk of the temperature effect is caused merely by the 300 K Fermi function cutoff which we show as the thin dark line in Fig. 7 overlaid on the 300 K spectrum. This was obtained by merely taking the fit to the 20 K spectrum and convoluting it with a 300 K Fermi function before instrument broadening. There is almost no room left for other effects, but we will still account for increased line shape broadening due to phonon effects at elevated temperatures. Also, while not needed to explain CeBe_{13} , shifts in the position of a narrow band cannot be totally excluded as the lattice parameter decreases with temperature, and we have already shown above how a change in position of the band can lead to drastic reductions in intensity. Thermal shifts as large as 60 meV have been observed in core levels³³ and valence band states of normal materials between 20–300 K. For now, however, we will ignore any shifts and consider only Fermi function and pho-

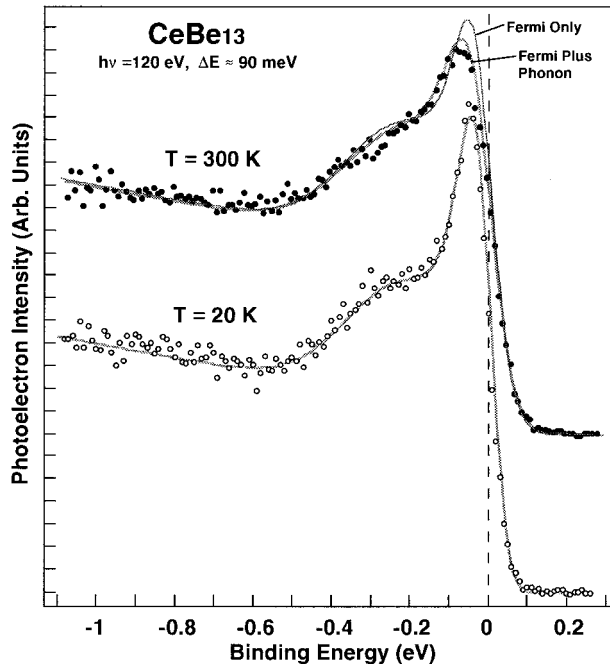


FIG. 7. CeBe_{13} spectra from a (110) surface at 20 K (same spectrum as in Fig. 5) and at 300 K. A fit was done to the 20 K spectrum, and the prebroadened components convoluted with a 300 K Fermi function to yield the thin line curve labeled Fermi only. The gray scale thick line at 300 K corresponds to first broadening the 20 K fit with a 100 meV Gaussian, to simulate phonon broadening, prior to convoluting with the Fermi function and instrument broadening.

non broadening which for $4f$ levels is typically reported as being of the order of 60 to 100 meV. Indeed, in our fits to the data of Patthey *et al.*¹⁷ we found that a phonon broadening of ≈ 90 meV (obtained from Si- $2p$ core levels) yielded good agreement with the data, both theirs and ours. Applying ≈ 100 meV of phonon broadening to CeBe_{13} (in Fig. 7) establishes that the $4f$ temperature dependence of CeBe_{13} can be entirely accounted for in both the $5/2$ and the $7/2$ components. This is accomplished by convoluting the unbroadened fitted spectrum at 20 K with a 100 meV (FWHM) Gaussian, cutting it by a 300 K Fermi function, and finally broadening it by the 90 meV instrument resolution. The resulting line shape is then superimposed on the 300 K spectrum of Fig. 7. As one can see, all the temperature dependence is completely accounted for with no need for additional mechanisms. Hence, there is no loss of spectral weight in the $4f_{5/2}$ at 300 K except for a small fraction (spectral weight change is 2%) due to the Fermi function cutoff of a broader $4f_{5/2}$ at 300 K. Thus the lack of a temperature dependence in XAS is understood and fully consistent with the PES data.

IV. DISCUSSION

The single impurity model, SIM, and its mathematical extensions to excitation spectra of Ce heavy fermions [GS (Refs. 2, 4, 6) and NCA (Ref. 6)] have lent insight into the final state transition probabilities observed in XPS and XAS spectroscopies of heavy fermions. In addition they have been highly successful in the interpretation of bulk property data such as magnetic susceptibility and specific heat. However,

with photoemission spectroscopy, a microscopic probe of the electronic structure, the model seems to run into difficulty. This difficulty is still obtained even upon the introduction of the periodic Anderson lattice⁴ (PAL) since most of the gross features of SIM should be retained in PAL, such as scaling of f^1 intensities with T_K , the temperature dependence, and indeed, the disappearance of the PAL and the singlet state upon heating above T_K where complete localization of the $4f$ s is assumed, and where a Curie-Weiss susceptibility is observed. By contrast, our previous results⁷ on CePt_{2+x} ($x \leq 1$) showed that amplitude modulation, interpreted as dispersion of the bands, is retained even up to $10T_K$ ($T_K \approx 10$ to 20 K), where the KR intensity should have been renormalized to zero. Moreover, the rationale⁶ for staying with SIM rather than PAL has been that the dispersion introduced by PAL would in any case be so small as to be imperceptible since it cannot be larger than T_K . The enormous amplitude differences in the $4f_{5/2}$ with momentum, on the other hand, suggest that the effects are large, and our line shape analyses suggest that the f -band crosses E_F , while the dispersion of the $4f_{7/2}$ sideband is at least three times larger than one would expect even within the PAL.

It has been suggested that the amplitude effect is merely a result of directional changes in coupling between the f electrons and the conduction band; i.e., the hybridization Δ should be written as $\Delta(k)$ and the physics of SIM is retained. But, this then implies that $T_K \rightarrow T_K(k)$ since within SIM the $4f_{5/2}$ amplitude is directly related to T_K . On the other hand, if T_K is still to be considered a thermodynamic quantity of a material, then the appearance of the $4f_{7/2}$ sideband at -325 meV in a high T_K material (vs typically -280 meV in a low T_K material) is exactly opposite to the predictions⁶ of NCA. This in any case still leaves unexplained the dispersion of the $4f_{7/2}$ and the f^0 peaks.

Besides dispersion, however, there are several other parameters to consider. We have performed a GS calculation (see Fig. 8) for a material with $T_K = 400$ K, a flat conduction band DOS having a width of 10 eV (even this may be too narrow since the Be- sp DOS peaks at -8 eV), and a Coulomb correlation energy U_{ff} of 14 eV. In Fig. 8 we compare it with a [110]-type spectrum (same spectrum as in Fig. 1, fresh cleave, but now broadened to the same resolution as the CePt_{2+x} spectrum) since it is closer in appearance to the calculation than the [100]-type spectra. Some of the disagreements, previously addressed by us,^{7,16,21,25-28,34} are enumerated below.

(i) To begin with, the ratio of the tetravalent to trivalent spectral weights (i.e., f^1/f^0) is calculated to be no more than 0.1. The actual values range from 0.3 to >1.0 , depending on direction, even after subtracting the d -electron contribution (see Fig. 2). Thus the “main” f^0 peak is much too small. This is mainly due to its small FWHM ≈ 1 eV (see Fig. 8) as opposed to the predicted 3–4 eV. However, the width of f^0 is nearly a constant for all Ce compounds irrespective of T_K . To emphasise the point we show in Fig. 8 a comparison of spectra for CeBe_{13} and CePt_{2+x} ($x \leq 1$). The spectral similarity is striking in view of the more than an order of magnitude difference in T_K 's. We make the further observation here that the f^0 peak always occurs in the vicinity of -2 eV. This is strange in view of the peaking of the Be-DOS at -8 eV where one would expect much stronger ligand hybridization.

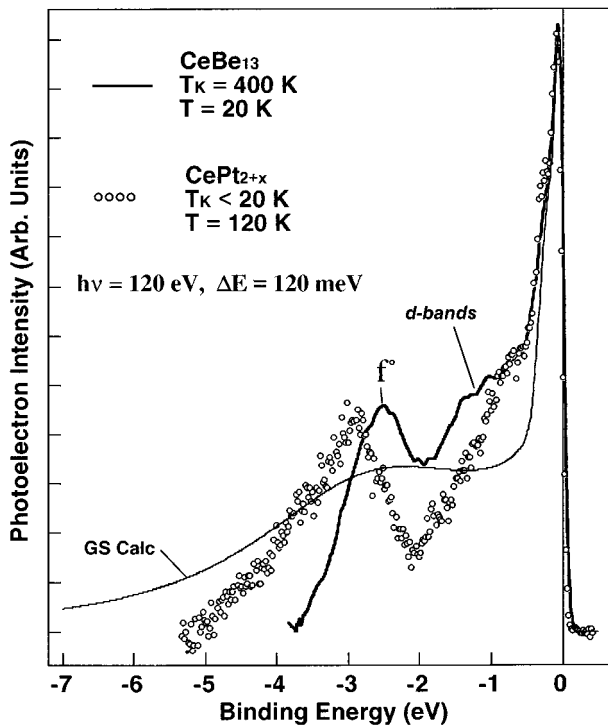


FIG. 8. Superposition of (110) spectrum from CeBe_{13} (same as in Fig. 1 but with background subtracted) with CePt_{2+x} spectrum from Ref. 7, and a GS calculated spectrum with parameters approximating CeBe_{13} (see text). Spectra were broadened as needed to match the Ref. 7 resolution, and normalized at the $4f_{5/2}$ peak. The T_K 's differ by an order of magnitude between the two materials. Note also the measurement temperatures.

It is our observation that the position of the f^0 peak is more closely associated with the bottom of the Ce-5d bands (i.e., at ≈ -2 eV), as first suggested by Riseborough,³⁵ and has less to do with ligand hybridization. It may legitimately be argued that the model DOS used in our calculation will not correctly reproduce the f^0 peak. However, our GS code reproduced quite accurately the calculated Kang *et al.*³⁵ spectrum of CeCu_2Si_2 using a flat DOS with their published parameters, despite the fact that the calculations of Kang *et al.* utilized a full band structure DOS. A more relevant parameter turned out to be the bandwidth.

(ii) The FWHM of the $4f_{5/2}$ is calculated to be 32 meV and has no crystal field levels. The actual value, as measured with 56 meV resolution, is 90 to 100 meV (lower limit) and is again nearly a constant for all materials irrespective of T_K .

(iii) The 0.1 eV dispersion of the "main" f^0 peak in Fig. 1 is difficult to reconcile within GS or NCA since this is the eigenvalue of the screened f level. Within a correlated band model, however, satellite dispersion may be possible,³⁶ as for example, in NiO.³⁷

(iv) There is no temperature dependence over and above conventional effects, as experimentally demonstrated here. In

a recent publication³⁸ it is stated that the lack of temperature dependence in Ce heavy fermion materials is a consequence of crystal field levels whose spectral weight is larger than the KR. However, the crystal field mechanism cannot be used in CeBe_{13} .

The bandlike nature of the $4f_{5/2}$, the lack of scaling with T_K , the lack of a temperature dependence of the $4f_{5/2}$ over and above conventional effects, all would suggest that an approach different from SIM may be called for. While the Kondo lattice approach may yet yield the necessary results, our present understanding suggests that it will not produce temperature independent bands far above T_K as demanded by our CePt_{2+x} data. While a number of theories have been proposed for heavy electron phenomena,^{1,2,39-43} any successful theory will have to simultaneously explain the very robust bands observed here, the lack of scaling with T_K , as well as correctly predict the unusual bulk properties of heavy electron systems, such as the enhanced, temperature independent susceptibility of CeBe_{13} below 200 K. We suspect that the primary ingredient is the narrow bandwidth. Several theories obtain this (see, for example, the renormalized band approach by Liu³⁹ in which the main mechanism for renormalization are charge fluctuations), but we focus on a recent paper by Sheng and Cooper⁸ who suggested a non-Kondo explanation for heavy fermion phenomena. Using a two-electron band theory they first do an exact two body treatment of the local correlations in a fashion similar to SIM, followed by hybridization interactions which give extended two-electron band states. Without invoking the concept of a Kondo resonance they are able to reproduce the wide diversity of magnetic and heavy fermion phenomena, including the enhanced susceptibility and specific heat, as well as correctly predict the Wilson ratio. Within this model the $4f$'s form narrow bands with only conventional temperature dependence, much as our data would suggest. While the understanding of this model is only in its early stages, it seems to contain the necessary properties indicated by our measurements over the past few years. Time will tell whether this model will stand up to careful scrutiny from the macroscopic end, but indications are that it is much better able to explain the diversity of phenomena and numerous transitions observed in heavy fermions. Like LDA, the Sheng-Cooper model in its simplest form fails to address the existence of the $4f_{7/2}$ feature as well as the f^0 peak (assuming it is non-zero) at ≈ -2.4 eV. However, as within most models^{36,43} these features can undoubtedly be obtained as screened f^{n-1} final state effects of the photoemission process.

ACKNOWLEDGMENTS

We wish to thank Professor B. Cooper for many helpful discussions, and for showing us his manuscript prior to publication.

We also wish to thank Dr. H.J. Park for assistance on the V4 beamline.

*Permanent address: National High Magnetic Field Laboratory, Florida State University, Tallahassee, FL 32306-4005.

¹J. M. Lawrence and D. M. Mills, *Comments Condens. Matter Phys.* **15**, 163 (1991). Also, see various articles in *The Handbook*

on the Physics and Chemistry of the Rare-Earths, edited by K. A. Gschneidner, Jr., L. Eyring, and S. Hufner (North-Holland, Amsterdam, 1987), Vol. 10.

²O. Gunnarson and K. Schönhammer, in *Handbook on the Physics*

- and *Chemistry of Rare Earths*, edited by K. A. Gschneider, Jr., L. Eyring, and S. Huffner (Elsevier Publishers, Amsterdam, 1987), Vol. 10, pp. 103–163.
- ³J. W. Allen, S.-J. Oh, O. Gunnarson, K. Schönhammer, M. B. Maple, M. S. Torikachvili, and I. Lindau, *Adv. Phys.* **35**, 275 (1986); J. W. Allen, in *Synchrotron Radiation Research: Advances in Surface and Interface Science, Volume I: Techniques*, edited by R. Z. Bachrach (Plenum, New York, 1992), pp. 253–323.
 - ⁴P. A. Lee, T. M. Rice, J. W. Serene, L. J. Sham, and J. W. Wilkins, *Comments Condens. Matter Phys.* **12**, 99 (1986).
 - ⁵O. Gunnarson and K. Schönhammer, *Phys. Rev. B* **31**, 4815 (1985); in *Theory of Heavy Fermions and Valence Fluctuations*, edited by T. Kasuya and T. Saso (Springer-Verlag, Berlin, 1986), p. 110.
 - ⁶N. E. Bickers, D. L. Cox, and J. W. Wilkins, *Phys. Rev. B* **36**, 2036 (1987).
 - ⁷A. B. Andrews, J. J. Joyce, A. J. Arko, J. D. Thompson, J. Tang, J. M. Lawrence, and J. C. Hemminger, *Phys. Rev. B* **51**, 3277 (1995).
 - ⁸Q. G. Sheng and B. R. Cooper, *Philos. Mag.* **72**, 123 (1995).
 - ⁹G. Krill, J. P. Kappler, M. F. Ravet, A. Amamou, and A. Meyer, *J. Phys. F* **10**, 1031 (1980).
 - ¹⁰E. Holland-Moritz, W. Weber, A. Severing, E. Zirngiebl, H. Spille, W. Baus, S. Horn, A. P. Murani, and J. L. Ragazzoni, *Phys. Rev. B* **39**, 6409 (1989).
 - ¹¹G. Borsa, *Phys. Status Solidi* **17**, 631 (1973).
 - ¹²J. P. Kappler and A. Meyer, *J. Phys. F* **9**, 143 (1980).
 - ¹³D. Wohlleben and J. Rohler, *J. Appl. Phys.* **55**, 1904 (1984).
 - ¹⁴K. Takegahara, H. Harima, and T. Kasuya, *J. Phys. F* **16**, 1691 (1986).
 - ¹⁵M. M. Steiner, R. C. Albers, and L. J. Sham, *Phys. Rev. Lett.* **72**, 2923 (1994).
 - ¹⁶J. M. Lawrence, A. J. Arko, J. J. Joyce, R. I. R. Blyth, R. J. Bartlett, P. C. Canfield, Z. Fisk, and P. S. Riseborough, *Phys. Rev. B* **47**, 15 460 (1993).
 - ¹⁷F. Patthey, W.-D. Schneider, Y. Baer, and B. Delley, *Phys. Rev. Lett.* **58**, 2810 (1987); F. Patthey, J.-M. Imer, W.-D. Schneider, H. Beck, and Y. Baer, *Phys. Rev. B* **42**, 8864 (1990).
 - ¹⁸U. Fano, *Phys. Rev.* **124**, 1886 (1961).
 - ¹⁹E. Weschke, C. Laubschat, T. Simmons, M. Domke, O. Strebel, and G. Kaindl, *Phys. Rev. B* **44**, 8304 (1991).
 - ²⁰C. Laubschat, E. Weschke, C. Holtz, M. Domke, O. Strebel, and G. Kaindl, *Phys. Rev. Lett.* **65**, 1639 (1990).
 - ²¹R. I. R. Blyth, J. J. Joyce, A. J. Arko, P. C. Canfield, Z. Fisk, J. D. Thompson, R. J. Bartlett, J. Tang, and J. M. Lawrence, *Phys. Rev. B* **48**, 9497 (1993).
 - ²²R. I. R. Blyth, A. B. Andrews, A. J. Arko, J. J. Joyce, P. C. Canfield, Z. Fisk, U. Lohia, and L. DeLong, *Surf. Rev. Lett.* **1**, 25 (1994).
 - ²³A. B. Andrews, J. J. Joyce, A. J. Arko, J. D. Thompson, Z. Fisk, J. Tang, J. M. Lawrence, P. S. Riseborough, and P. C. Canfield, *Physica B* **206&207**, 83 (1995).
 - ²⁴*Pearson's Handbook of Crystallographic Data*, edited by P. Villars and L. D. Calvert (Materials Information Society, Materials Park, OH, 1991), p. 1271.
 - ²⁵J. J. Joyce, A. J. Arko, A. B. Andrews, and R. I. R. Blyth, *Phys. Rev. Lett.* **72**, 1774 (1994).
 - ²⁶J. J. Joyce, A. J. Arko, J. M. Lawrence, P. C. Canfield, Z. Fisk, R. J. Bartlett, and J. D. Thompson, *Phys. Rev. Lett.* **68**, 236 (1992).
 - ²⁷J. J. Joyce, A. J. Arko, R. J. Bartlett, P. Canfield, Z. Fisk, and J. Lawrence, *Bull. Am. Phys. Soc.* **36**, 460 (1991).
 - ²⁸J. J. Joyce and A. J. Arko, *Phys. Rev. Lett.* **70**, 1181 (1993).
 - ²⁹D. Malterre, M. Grioni, P. Weibel, and Y. Baer, *Phys. Rev. Lett.* **68**, 2656 (1992).
 - ³⁰L. H. Tjeng, S.-J. Oh, E.-J. Cho, H.-J. Lin, C. T. Chen, G.-W. Gweon, J.-H. Park, J. W. Allen, T. Suzuki, M. S. Makivic, and D. L. Cox, *Phys. Rev. Lett.* **71**, 1419 (1993).
 - ³¹G. Kaindl, G. Kalkowski, W. D. Brewer, E. V. Sampathkumaran, F. Holtzberg, and A. Schach v. Wittenau, *J. Magn. Magn. Mater.* **47&48**, 181 (1985).
 - ³²J. M. Lawrence, G. H. Kwei, P. C. Canfield, J. G. DeWitt, and A. C. Lawson, *Phys. Rev. B* **49**, 1627 (1994).
 - ³³D. M. Riffe, G. K. Wetheim, D. N. E. Buchanan, and P. H. Citrin, *Phys. Rev. B* **45**, 6216 (1992).
 - ³⁴J. J. Joyce, A. J. Arko, J. M. Lawrence, P. C. Canfield, R. J. Bartlett, Z. Fisk, J. D. Thompson, and J. Tang, *Solid State Commun.* **83**, 551 (1992); A. B. Andrews, R. I. R. Blyth, A. J. Arko, J. J. Joyce, Z. Fisk, J. D. Thompson, R. J. Bartlett, P. C. Canfield, C. G. Olson, P. Benning, and P. S. Riseborough, *Physica B* **199&200**, 15 (1994).
 - ³⁵J.-S. Kang, J. W. Allen, Y. Lassailly, M. B. Maple, and M. S. Torikachvili, *Phys. Rev. B* **41**, 6610 (1990).
 - ³⁶P. S. Riseborough, *Solid State Commun.* **57**, 721 (1986).
 - ³⁷Z.-X. Shen, R. S. List, D. S. Dessau, A. J. Arko, R. J. Bartlett, O. Jepsen, B. O. Wells, and F. Parmigiani, *Solid State Commun.* **79**, 623 (1991).
 - ³⁸Stefan Huffner, *Photoelectron Spectroscopy, Principles and Applications*, Springer Series in Solid State Sciences Vol. 82 (Springer-Verlag, Berlin, 1995), pp. 104–111.
 - ³⁹S. H. Liu, in *Handbook on the Physics and Chemistry of Rare Earths*, edited by K. A. Gschneider and L. Eyring (North-Holland, Amsterdam, 1993), Vol. 17, Chap. 111, pp. 87–148.
 - ⁴⁰Gertrud Zwicknagl, *Adv. Phys.* **41**, 203 (1992).
 - ⁴¹M. M. Sanchez-Lopez, J. Costa-Quintana, E. Gonzales-Leon, F. Lopez-Aguilar, and L. Puig-Puig, *Physica B* **199&200**, 202 (1994).
 - ⁴²Tadao Kasuya, *JJAP Ser.* **8**, 3 (1993).
 - ⁴³M. R. Norman, *Phys. Rev. B* **31**, 6261 (1985); M. R. Norman, D. D. Koelling, and A. J. Freeman, *ibid.* **31**, 6251 (1985).